

Article

PAPR Suppression for Angular-Domain-Based Massive Multiple-Input Multiple-Output Orthogonal Frequency Division Multiplexing System

Ting Liu ^{1,*}, Xiaoming Wang ², Yuanxue Xin ³ and Xi Yang ⁴

¹ School of Artificial Intelligence, Nanjing University of Information Science and Technology, Nanjing 210044, China

² School of Communication & Information Engineering, Nanjing University of Posts and Telecommunications, Nanjing 210003, China; xmwang@njupt.edu.cn

³ School of Information Science and Engineering, Hohai University, Changzhou 213000, China; xinyx@hhu.edu.cn

⁴ Shanghai Key Laboratory of Multidimensional Information Processing, School of Communication and Electronic Engineering, East China Normal University, Shanghai 200241, China; xyang@cee.ecnu.edu.cn

* Correspondence: liuting@nuist.edu.cn

Abstract: In this paper, the precoding-based peak-to-average power ratio (PAPR) reduction methods are studied for the massive multiple-input multiple-output (MIMO) orthogonal frequency division multiplexing (OFDM) system in the angular domain. The expectation maximization generalized approximate message passing algorithm and the proposed optimized alternating direction method of multipliers (OADMM) scheme are adopted here to explore the system characteristics in terms of the symbol error ratio (SER) performance, the PAPR reduction efficiency, and the inter user interference (IUI). Specifically, the high PAPR problem is reduced to no more than 0.18 dB by using the inherent property of the massive MIMO-OFDM angle division multiple access (ADMA) system with relatively reduced computational complexity. Moreover, the value of SER is around 10^{-5} dB when the proposed technique is performed. Computer numerical simulation results verify the efficiency of the proposed technique from the perspective of SER, PAPR suppression, and IUI.

Keywords: PAPR reduction; precoding; ADMA; Massive MIMO-OFDM



Citation: Liu, T.; Wang, X.; Xin, Y.; Yang, X. PAPR Suppression for Angular-Domain-Based Massive Multiple-Input Multiple-Output Orthogonal Frequency Division Multiplexing System. *Electronics* **2023**, *12*, 4015. <https://doi.org/10.3390/electronics12194015>

Academic Editor: David A. Sánchez-Hernández

Received: 26 August 2023

Revised: 18 September 2023

Accepted: 22 September 2023

Published: 23 September 2023



Copyright: © 2023 by the authors. Licensee MDPI, Basel, Switzerland. This article is an open access article distributed under the terms and conditions of the Creative Commons Attribution (CC BY) license (<https://creativecommons.org/licenses/by/4.0/>).

1. Introduction

Massive multiple-input multiple-output (MIMO) is a key technology in the fifth-generation (5G) and the sixth-generation (6G) mobile communication systems [1–3]. In the large-scale MIMO system, the base station (BS) deploys antenna arrays with tens to hundreds of elements. As a result, there is a noticeable improvement in the frequency, energy efficiency, spatial resolution, and spatial resource usage. In [4], the advantages of massive MIMO in the low-frequency bands were investigated by the authors without regard to the spatial limitations. In [5], the dynamic metasurface antennas were a desirable technology for the extremely massive MIMO transceiver of sixth-generation (6G) wireless networks due to their flexible antenna topologies with a significant number of components of decreased size and hardware costs. To increase the transmission and receiver efficiency of the 6G communications systems, the authors in [6] explored the cell-free massive MIMO technique. Specifically, a power control theory was proposed in [7] to accomplish the practical deployment of the cell-free massive MIMO for the internet of everything of 6G networks. Additionally, in [8], the characteristics of the unmanned aerial vehicle channels were investigated in the 6G massive MIMO millimeter wave system. Particularly, the transformer deep learning framework was employed to explore the massive MIMO semantic communication system [9]. Furthermore, the fundamentals, channel modeling, and system analysis of massive MIMO were also demonstrated in [10–12]. The potential

of massive MIMO to reuse the space may be leveraged to create generalized transmission systems exploiting multiple access transmission technologies, such as the beam division multiple access (BDMA) [13–15]. In [16], the hybrid precoding technique of the BDMA THz communication was proposed to eliminate inter-beam interference. For the quality of service, the authors of [17] designed a unique multiple-beam access system and a power allocation method. In [18], the spatial division multiple access system's throughput was shown to be improved by the beam selection and aggregation approach. Additionally, the beam training and allocation were studied with the purpose of providing huge connectivity with lower packet loss [19]. Moreover, the joint spatial division multiplexing (JSDM) and the angle division multiple access (ADMA) schemes were also investigated in [20–22].

ADMA is a signal transmission technology for angular domain signals that fully exploits the characteristics of the channel [23,24]. Because of the sparsity of terminal distributions, the spatial channel state information (CSI) can be mapped onto the beam domain, which results in a reduction in the channel matrix's size. Additionally, the angle of arrival (AoA) in ADMA may be accurately calculated by further reducing the size of the channel matrix. Reduced training overhead, and multipath fading resistance in the massive MIMO orthogonal frequency division multiplexing (OFDM) ADMA system as a result, increase the spatial resolution and resource utilization.

There are many methods to control the high peak-to-average power ratio (PAPR) in the OFDM systems, including but not limited to clipping, tone reservation, tone injection, and so on [25–27]. To lower the PAPR, the authors of [28] presented a parameter optimization approach for signal linear scaling. In [29], a novel waveform-designing algorithm was proposed to reduce the PAPR of the integrated radar and wireless communication system. Further research was conducted regarding the partial transmit sequence method to reduce the high PAPR of the OFDM system [30]. An adaptive technique to reduce the PAPR in the OFDM system was put out in [31] with reduced bit error ratio deterioration. In [32], the authors summarized the currently available PAPR reduction methods and optimized the PAPR by employing wavelet clipping and compounding. However, in the scenario of the massive multiuser MIMO-OFDM, the computational complexity of the aforementioned conventional approaches exponentially increases. Fortunately, reasonably affordable antenna reservation and adaptive tone reservation techniques have already been developed. Moreover, the constant envelope precoding techniques were adopted in [33,34], and a factor-graph-based approximate message passing (AMP) precoding technique was also proposed to decrease the high PAPR and multiuser inference [35,36]. In the massive MIMO-OFDM-ADMA system, particularly for the downlink transmission, the issue of the high peak-to-average power ratio (PAPR) also has to be resolved. The baseband transmit signals' amplitude values fall within a relatively wide range, and specifically, all signals from all beams at the transmitter are added following the inverse transformation in the angular domain. As a result, the huge multiuser MIMO-OFDM-ADMA system is facing a critical problem: how can the PAPR be lowered with minimal complexity?

In this paper, in order to reduce the high PAPR in the massive multiuser MIMO-OFDM-ADMA system, the expectation maximization (EM) truncation Gaussian mixture (TGM) generalized AMP (GAMP) algorithm [37] is employed as the joint precoding scheme. Additionally, an optimized alternating direction method of multipliers (ADMM) algorithm is also proposed for the PAPR reduction. The two joint precoding approaches mentioned above perform very well in simulations with regard to PAPR reduction, symbol error ratio (SER), and interuser interference (IUI) for the massive multiuser MIMO-OFDM system in the angular domain.

2. System Model

Suppose a downlink massive multiuser MIMO-OFDM signal transmission scenario with M BS antennas in the angular domain. There are K single-antenna users served by one BS, and the number of subcarriers is N . It is assumed that the channel angular index set $I_{k,n}^{ro}$, the rotation parameter $\phi_{k,n}^{ro}$, the downlink CSI $\mathbf{h}_{k,n}^T$, and the downlink CSI in the

angular domain $\mathbf{h}_{k,n}^{-T}$ are known at the BS. The g -th group index is defined as U_g with $K_g = |U_g|$ users in each group, and $g = 1, \dots, G$. Suppose a frequency selective fading channel propagation environment, and the received signal is expressed as

$$\mathbf{Y} = \mathbf{H}\mathbf{X} + \mathbf{N} \tag{1}$$

where $\mathbf{X} = [\mathbf{x}_0, \dots, \mathbf{x}_m, \mathbf{x}_{M-1}]^T$ with $\mathbf{x}_m \in \mathbb{C}^N$ being signal at the m -th antenna; $\mathbf{Y} = [\mathbf{y}_0, \dots, \mathbf{y}_n, \mathbf{y}_{N-1}]^T \in \mathbb{C}^{K_g \times N}$ is the received signal, and $\mathbf{y}_n \in \mathbb{C}^{K_g}$ is the received signal of the n -th subcarrier; \mathbf{N} is the noise signal with variance σ^2 ; $\mathbf{H} = \mathbf{G}\mathbf{F}_1\mathbf{P}\mathbf{F}_2$, and $\mathbf{G} = \text{diag}(\mathbf{H}_0, \mathbf{H}_1, \dots, \mathbf{H}_{N-1}) \in \mathbb{C}^{KN \times MN}$ is the angular-domain channel matrix with $\mathbf{H}_n = [\bar{\mathbf{h}}_{1,n}^{-T}, \bar{\mathbf{h}}_{2,n}^{-T}, \dots, \bar{\mathbf{h}}_{K_g,n}^{-T}]^T \in \mathbb{C}^{K_g \times M}$, $\mathbf{F}_1 = \text{diag}(\mathbf{F}_{M,0}^H, \dots, \mathbf{F}_{M,N-1}^H)$ as the expanding inverse discrete Fourier transform (IDFT) matrix, and $\mathbf{F}_{M,n}^H = [\mathbf{f}_{0,n}, \mathbf{f}_{1,n}, \dots, \mathbf{f}_{M-1,n}] \in \mathbb{C}^{M \times M}$. Specifically, $\mathbf{f}_{i,n} = \mathbf{\Phi}(\bar{\phi}_{l,n})^H \mathbf{f}'_i$, where \mathbf{f}'_i is the i -th column of the IDFT matrix, $\mathbf{\Phi}(\bar{\phi}_{l,n}) = \text{diag}(1, e^{j\bar{\phi}_{l,n}}, \dots, e^{j(M-1)\bar{\phi}_{l,n}})$ is the angular rotation matrix, and $\bar{\phi}_{l,n}$ is the angular rotation factor corresponding to the l -th column of IDFT matrix on the n -th subcarrier. Equation (2) gives the definition of $\bar{\phi}_{l,n}$, which is

$$\bar{\phi}_{l,n} = \begin{cases} \phi_{k,n}, & l \in I_{k,n}^{ro}, k \in U_g \\ 0, & l \notin I_{k,n}^{ro}, k \in U_g \end{cases} \tag{2}$$

where $\phi_{k,n}$ is the angular rotation factor of the k -th user on the n -th subcarrier. The permutation matrix is $\mathbf{P} \in \mathbb{C}^{MN \times MN}$, and the element of \mathbf{P} in the a_1 -th row and the a_2 -th column is

$$[\mathbf{P}]_{a_1 a_2} = \begin{cases} 1, & \text{floor}(a_1/M \text{ or } N) = \text{mod}(a_2, \text{Nor}M) \\ 0, & \text{else} \end{cases} \tag{3}$$

The expanded transform matrix is $\mathbf{F}_2 = \text{diag}(\mathbf{F}, \dots, \mathbf{F}) \in \mathbb{C}^{MN \times MN}$, where $\mathbf{F} \in \mathbb{C}^{N \times N}$ is the discrete Fourier transform (DFT) matrix.

3. PAPR Reduction in the Angular Domain

Firstly, define

$$\mathbf{S} = \mathbf{H}\mathbf{X}, \tag{4}$$

as the precoding constrains of \mathbf{X} in order to the eliminate the multiuser interference. Then, the received signal can be rewritten as

$$\mathbf{Y} = \mathbf{S} + \mathbf{N}. \tag{5}$$

Consequently, the PAPR reduction in \mathbf{X} can be considered as a convex problem due to the underdetermined property of Equation (4). That is,

$$\begin{aligned} \min_{\mathbf{X}} \quad & \|\mathbf{X}\|_{\infty} \\ \text{s.t.} \quad & \mathbf{S} = \mathbf{H}\mathbf{X} \end{aligned} \tag{6}$$

where $\|\cdot\|_{\infty}$ is the infinite norm.

3.1. EM-TGM-GAMP

For the purpose of tackling the PAPR reduction problem in the massive multiuser MIMO-OFDM-ADMA system, we first apply the EM-TGM-GAMP algorithm. To estimate the joint likelihood probability function $p(\mathbf{Y}|\mathbf{X})$ in this framework, the GAMP algorithm is integrated into the variational architecture of the EM algorithm. As is well known, the GAMP algorithm is a simplified version of the loopy basis pursuit. It is often used to approximate the likelihood and the marginal posteriors. Here, the GAMP scheme is applied to make an iterative estimation of the likelihood function $p(\mathbf{Y}|\mathbf{X})$, i.e., $\hat{p}(\mathbf{Y}|\mathbf{X})$.

Then, the variational EM method gives the new estimators of \mathbf{X} and the corresponding noise variance simultaneously. The main idea of the angular domain EM-TGM-GAMP algorithm is depicted in Figure 1, and the whole iteration procedure is shown in Algorithm 1. Specifically, the iterative update procedure of parameter ζ is given by [37].

$$\zeta^{t+1} = \zeta^t + \frac{(\mathbf{Y} - \mathbf{H}\hat{\mathbf{X}})^T \mathbf{H}}{\|\mathbf{H}\|_2^2}. \tag{7}$$

where t is the iteration index.

Algorithm 1: EM-TGM-GAMP-ADMA

Input: $\mathbf{S}, \mathbf{H}, \mathbf{Y}, T$

Initialize: $t = 0, \zeta = \|\mathbf{Y}\|_\infty / \|\mathbf{H}\|_\infty$

While $t \leq T$ **do**

1. Estimate the posterior distributions $\hat{p}(\mathbf{Y}|\mathbf{X})$ and $\hat{p}(\mathbf{S}|\mathbf{Y})$ using GAMP algorithm;
2. Make a posterior estimation of \mathbf{X} to obtain $\hat{\mathbf{X}}$ based on the likelihood approximation $\hat{p}(\mathbf{Y}|\mathbf{X})$;
3. Compute the estimator of noise variance using EM procedure, and update the value of ζ to minimize $\|\mathbf{Y} - \mathbf{H}\hat{\mathbf{X}}\|_2^2$;

Output: $\hat{\mathbf{X}} = \mathbf{X}^{t+1}$.

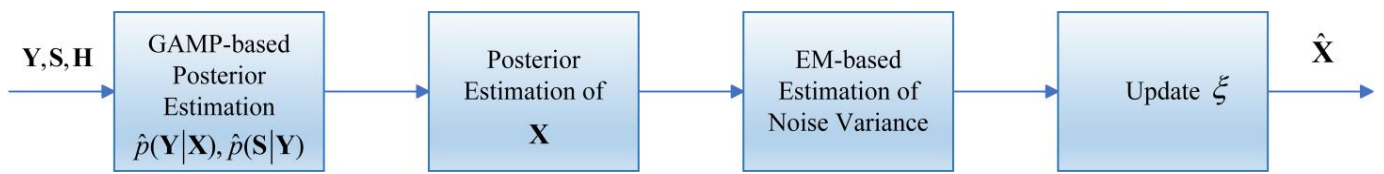


Figure 1. The flow diagram of Algorithm 1.

3.2. Optimized ADMM

The fact that Algorithm 1 requires numerous vector multiplications is important to note. And the optimized ADMM is therefore proposed in the following. In order to reduce the PAPR, the signal \mathbf{X} is supposed to be restricted in set \mathcal{A} . Moreover, the objective function is given by

$$\begin{aligned} \min_{\mathbf{X}, \alpha} & \|\mathbf{S} - \alpha \mathbf{H}\mathbf{X}\|_2^2 + \alpha^2 K_g \sigma^2 \\ \text{s.t.} & \mathbf{X} \in \mathcal{A}, \alpha > 0 \end{aligned}, \tag{8}$$

where α is the precoding parameter. Notably, the elements of the set \mathcal{A} can be designed in the rings, the circles, or the finite element sets. From the perspective of ADMM algorithm, we obtain

$$\begin{aligned} \min_{\mathbf{X}_1, \mathbf{X}} & \|\mathbf{S} - \mathbf{H}_1 \mathbf{X}_1\|_2^2 + I_{\mathcal{A}}(\mathbf{X}) \\ \text{s.t.} & \mathbf{X}_1 - \mathbf{X} = \mathbf{0} \end{aligned}, \tag{9}$$

where $\mathbf{H}_1 = \alpha \mathbf{H}$, $I_{\mathcal{A}}(\cdot) = 0$ when $\mathbf{X} \in \mathcal{A}^M$. The module diagram of the optimized ADMM-ADMA scheme is illustrated in Figure 2, and the iteration steps of the proposed proposal are summarized in Algorithm 2.

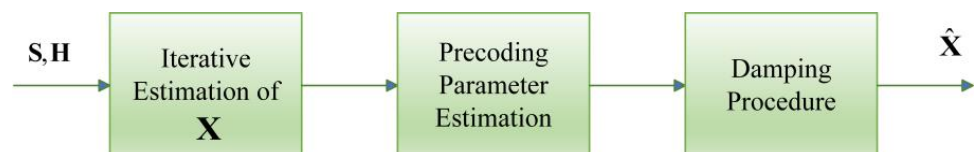


Figure 2. The flow diagram of Algorithm 2.

Algorithm 2: Optimized ADMM-ADMA

Input: $\mathbf{S}, \mathbf{H}, \Lambda_1 = \{\text{diag}(\mathbf{H}^H \mathbf{H})\}^{-1} \mathbf{H}^H, T_1, T_2$

Initialize: $t = 0, \mathbf{X}^0 = \mathbf{0}, \alpha^0 = 1, \rho = 0.90$

While $t \leq T_1$ **do**

1. $\mathbf{X}^{t+1} = \prod_{\mathcal{A}^M} \{\mathbf{X}^t + \Lambda_1(\frac{1}{\alpha^t} \mathbf{S} - \mathbf{H}_1 \mathbf{X}^t)\};$

2. If $\text{mod}(T_2, t + 1) == 0$
 $\alpha^{t+1} = \frac{\text{Re}(\mathbf{S}^H \mathbf{H} \mathbf{X}^{t+1})}{\|\mathbf{H} \mathbf{X}^{t+1}\|_2^2 + K_s \sigma^2};$

else

$\alpha^{t+1} = \alpha^t;$

3. $\mathbf{X}^{t+1} = \rho \mathbf{X}^t + (1 - \rho) \mathbf{X}^{t+1};$

4. $t = t + 1;$

Output: $\hat{\mathbf{X}} = \mathbf{X}^{t+1}.$

Define the Lagrangian function of (9) as

$$F(\mathbf{X}_1, \mathbf{X}, \mathbf{D}) = \|\mathbf{S} - \mathbf{H}_1 \mathbf{X}_1\|_2^2 + I_{\mathcal{A}}(\mathbf{X}) + \mathbf{D}^H (\mathbf{X}_1 - \mathbf{X}) + \eta \|\mathbf{X}_1 - \mathbf{X}\|_2^2, \tag{10}$$

where \mathbf{D} is the dual factor, and η is the Lagrangian parameter. The iterative steps are given by

$$\mathbf{X}_1^{t+1} = \underset{\mathbf{X}_1}{\text{argmin}} F(\mathbf{X}_1, \mathbf{X}^t, \mathbf{D}^t), \tag{11}$$

$$\mathbf{X}^{t+1} = \underset{\mathbf{X}}{\text{argmin}} F(\mathbf{X}_1^{t+1}, \mathbf{X}, \mathbf{D}^t), \tag{12}$$

$$\mathbf{D}^{t+1} = \mathbf{D}^t + \eta (\mathbf{X}_1^{t+1} - \mathbf{X}^{t+1}). \tag{13}$$

Then, we obtain

$$\mathbf{X}_1^{t+1} = \mathbf{X}^t + \Lambda (\mathbf{S} - \mathbf{H}_1 \mathbf{X}^t), \tag{14}$$

where $\Lambda = (\mathbf{H}_1^H \mathbf{H}_1 + \eta^t \mathbf{I})^{-1} \mathbf{H}_1^H$. Consider an arbitrary channel model as follows:

$$\mathbf{S} = \mathbf{H}_1 \mathbf{X} + \mathbf{W}, \tag{15}$$

where $\mathbf{W} \sim \mathcal{CN}(\mathbf{0}, \mathbf{I})$. Then, the linear estimation is given by

$$\hat{\mathbf{X}} = \Lambda \mathbf{S} + \mathbf{B}, \tag{16}$$

where

$$\Lambda = \mathbf{C}_{\mathbf{X}\mathbf{S}} \mathbf{C}_{\mathbf{S}}^{-1}, \tag{17}$$

$$\mathbf{B} = \hat{\mathbf{X}} - \Lambda \hat{\mathbf{S}}, \tag{18}$$

are computed by minimizing the expectation of $E\{(\mathbf{X} - \mathbf{X}^t)(\mathbf{X} - \mathbf{X}^t)^H\}$. Moreover, $\hat{\mathbf{X}}$ is the expectation of \mathbf{X} , $\hat{\mathbf{S}}$ is the expectation of \mathbf{S} , $\mathbf{C}_{\mathbf{X}\mathbf{S}}$ is the covariance matrix between \mathbf{X} and \mathbf{S} , and $\mathbf{C}_{\mathbf{S}}$ is the covariance result of \mathbf{S} .

Next, we have

$$\mathbf{C}_{\mathbf{X}\mathbf{S}} = \mathbf{C}_{\mathbf{X}} \mathbf{H}_1^H, \tag{19}$$

$$\mathbf{C}_{\mathbf{S}} = \mathbf{H}_1 \mathbf{C}_{\mathbf{X}} \mathbf{H}_1^H + \mathbf{C}_{\mathbf{W}}, \tag{20}$$

where $\mathbf{C}_{\mathbf{X}}$ is the covariance of \mathbf{X} . Then, Λ and \mathbf{B} are given by

$$\Lambda = (\mathbf{H}_1^H \mathbf{H}_1 + \eta^t \mathbf{I})^{-1} \mathbf{H}_1^H, \tag{21}$$

$$\mathbf{B} = \mathbf{X}^t - \Lambda \mathbf{H}_1 \mathbf{X}^t. \tag{22}$$

Finally, an optimal linear MMSE estimation is given by

$$\hat{\mathbf{X}} = \mathbf{X}^t + \Lambda(\mathbf{S} - \mathbf{H}_1 \mathbf{X}^t), \tag{23}$$

and $E\{\hat{\mathbf{X}}\} = (\mathbf{I} - \Lambda \mathbf{H}_1) \mathbf{X}^t + \Lambda \mathbf{H}_1 E\{\mathbf{X}\}$. As a consequence, the iterative procedures are provided by

$$\mathbf{X}^{t+1} = \prod_{\mathcal{A}} \{\mathbf{X}^t + \Lambda_1(\mathbf{S} - \mathbf{H}_1 \mathbf{X}^t)\}, \tag{24}$$

$$\mathbf{X}^{t+1} = \rho \mathbf{X}^t + (1 - \rho) \mathbf{X}^{t+1}, \tag{25}$$

where ρ is the damping factor, $\Lambda_1 = \{\text{diag}(\Lambda \mathbf{H}_1)\}^{-1} \Lambda$, and η is given by

$$(\eta^t)^{-1} = \frac{\|\mathbf{S} - \mathbf{H}_1 \mathbf{X}^t\|_2^2}{\text{tr}(\mathbf{H}_1^H \mathbf{H}_1)}, \tag{26}$$

where $\text{tr}(\mathbf{H}_1^H \mathbf{H}_1)$ is the normalization factor.

Furthermore, α is optimized as follows when \mathbf{X} remains unchanged

$$\begin{aligned} \min_{\alpha} \quad & \|\mathbf{S} - \alpha \mathbf{H} \mathbf{X}\|_2^2 + \alpha^2 K_g \sigma^2, \\ \text{s.t.} \quad & \alpha > 0 \end{aligned} \tag{27}$$

and α is given by

$$\alpha = \frac{\text{Re}(\mathbf{S}^H \mathbf{H} \mathbf{X})}{\|\mathbf{H} \mathbf{X}\|_2^2 + K_g \sigma^2}. \tag{28}$$

3.3. Computational Complexity Analysis

It is noted that EM-TGM-GAMP has the computational complexity on the order of $O(KN)$, mostly due to the multiplication of vector and matrix at each iteration. The computational complexity of the optimized ADMM algorithm is on the order of $O(2MK + M)$ at each iteration. The iterations (i.e., T_2) are necessary to improve the performance improvement of the proposed scheme. However, when T_2 is decreased, the performance curves may fluctuate. To put it another way, the iteration number has to be set up properly to boost the system performance while requiring less computing effort.

4. Numerical Results

In this section, the framework of antenna is assumed to be the uniform linear array (ULA), and the interval of antenna equals to $\lambda/2$. The number of OFDM subcarrier is 128 or 256. It is supposed that all users are uniformly distributed and served by the BS at the same time-frequency resource. The frequency channel response $\mathbf{H}_{f,n}$ of each subcarrier n is given by

$$\mathbf{H}_{f,n} = \sum_{p=0}^{P-1} \mathbf{H}_{t,p} e^{-j \frac{2\pi}{N} p n}, \tag{29}$$

where $\mathbf{H}_{t,p}$ is the channel response in the time domain, and the number of channel taps is $P = 8$.

In Figures 3 and 4, the number of subcarriers is indicated as 128 and 256, respectively. The values of SER are shown to decrease as the number of subcarriers increases. Figure 3 demonstrates the SER versus the signal-to-noise ratio (SNR) when both the quadrature phase shift keying (QPSK) and the 16-quadrature amplitude modulation (QAM) are considered, and the BS is equipped with different antennas. The constant envelope precoding is taken into account, with the elements of \mathcal{A} uniformly distributed in a unit circle. It is shown that the SER performance improvement of Algorithm 2 is fairly noticeable when M

varies from 16 to 64. Moreover, the SER performance of Algorithm 2 is better than that of Algorithm 1, especially in the regime of low SNR. For instance, the SER of Algorithm 2 is about 0.54 dB lower than that of the Algorithm 1 under the QPSK modulation when SNR equals 10 dB and $M = 64$. Moreover, the SER of Algorithm 2 with 64 antennas established at the BS is around 1.86×10^{-5} dB when SNR rises to 30 dB. However, for Algorithm 1 with QPSK modulation, the value of SER is about 3×10^{-4} dB. Figure 3 also depicts the SER performance of different schemes under the circumstance of the 16QAM. As expected, the SER of Algorithm 2 with 64 antennas at the BS is reduced by 0.04 dB when compared to the framework with 32 antennas established at the BS. Notably, the SER performance of Algorithm 1 with 64 antennas is worse than that of the Algorithm 2 with 16 antennas at the BS.

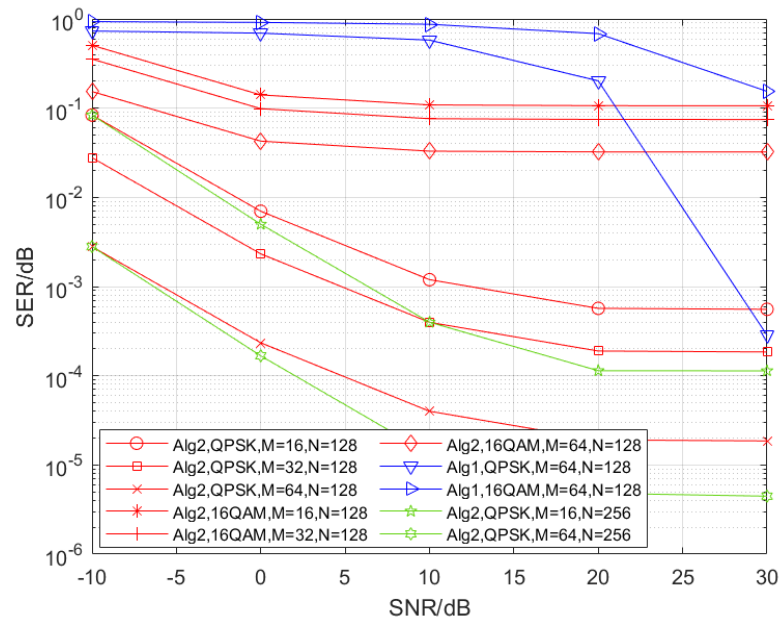


Figure 3. SER versus SNR for different PAPR reduction schemes.

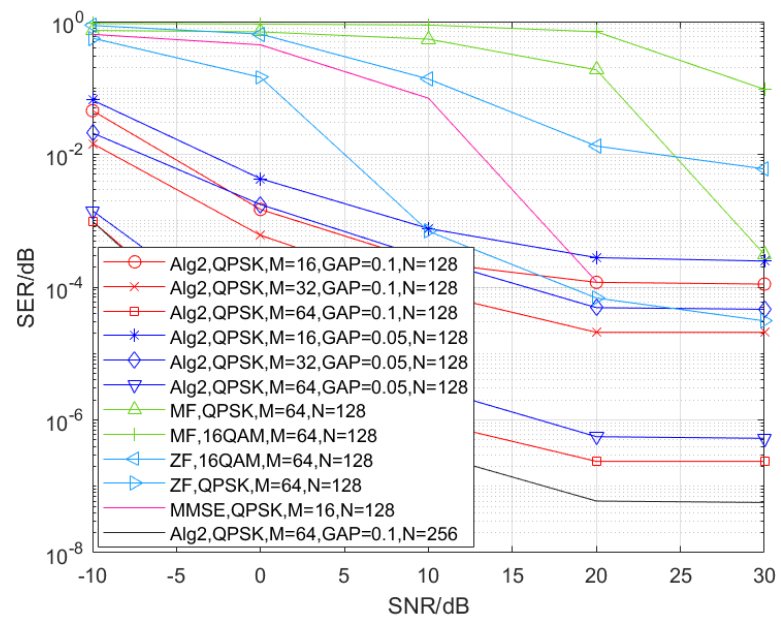


Figure 4. SER versus SNR for the AC-based precoding method.

The annulus constrained precoding is designed in Figure 4, and the elements of \mathcal{A} are uniformly distributed in three concentric circles. The values of the radius length of these three concentric circles are assumed to be 0.9, 1.0, and 1.1 with $\text{GAP} = 0.1$, and 0.95, 1.0, and 1.05 with $\text{GAP} = 0.05$, respectively. As expected, regardless of whether the value of GAP is equal to 0.1 or 0.05, the SER performance of Algorithm 2 improves dramatically as the number of BS antennas grows from 16 to 64. Furthermore, Figure 4 demonstrates that for a given number of BS antennas, the values of SER with $\text{GAP} = 0.1$ are lower than those with $\text{GAP} = 0.05$. Additionally, it should be pointed out that under conditions of small SNR (SNR below 10 dB), there is little difference in SER performance between $M = 16$, $\text{GAP} = 0.1$ and $M = 32$, $\text{GAP} = 0.05$. Particularly, the value of SER can almost arrive at 10^{-7} under the modulation of QPSK when $\text{GAP} = 0.1$, $\text{SNR} = 20$ dB, and $M = 64$. As well, it is discovered that the value of SER is less than 10^{-6} when $\text{GAP} = 0.05$, while SNR and M remain unchanged. Figure 4 also depicts the SER performance using matched filtering (MF), zero forcing (ZF), and traditional MMSE methods. It is observed that the SER performance of MF and ZF is worse than that of Algorithm 2. Specifically, the traditional MMSE scheme is close to that of Algorithm 2 in the regime of high SNR. However, it is acquired at the high cost of PAPR suppression performance.

Figure 5 demonstrates the PAPR reduction performance of Algorithm 1 and the MF scheme when $M = 64$ under QPSK modulation. It is shown that neither technique's PAPR performance is up to par. To be specific, all values of PAPR in Figure 5a fall around between 2.4 dB and 4 dB when Algorithm 1 is adopted here. Figure 5b contrasts this with the values of PAPR obtained using the MF method, which have a probability higher than 0.9 and fall between 8 dB and 12 dB. That is to say, it is impossible to achieve the tradeoff between PAPR reduction and SER performance using these two schemes.

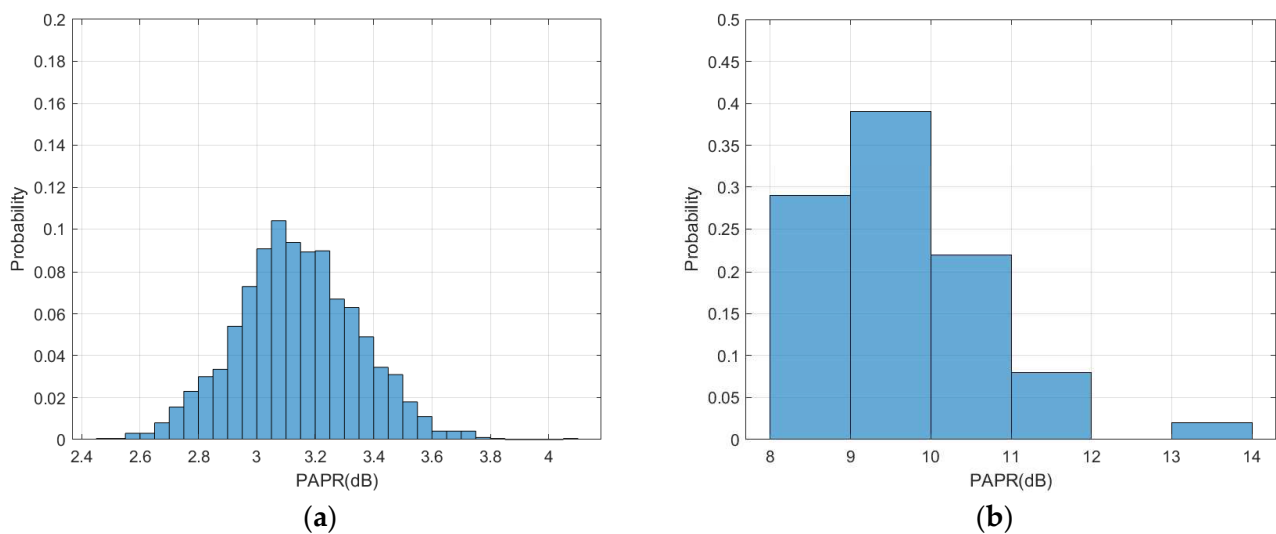


Figure 5. PAPR performance of Algorithm 1 and MF method under QPSK when $M = 64$. (a) Algorithm 1; (b) MF scheme.

Figure 6 illustrates the PAPR and the interuser interference (IUI) performance of Algorithm 2 when $M = 64$ and QPSK and 16 QAM are used for modulation. It is observed in Figure 4 that the proposed Algorithm 2 reduces PAPR in a suitable manner and improves the IUI performance in Figure 6a,b. Specifically, the values of PAPR are smaller than 0.15 dB with a probability greater than 0.95 in Figure 6a. In Figure 6b, the values of IUI ranges from -25 dB to -10 dB as well. This means that the proposed technique achieves a favorable trade off in terms of SER, PAPR reduction, and the IUI performance.

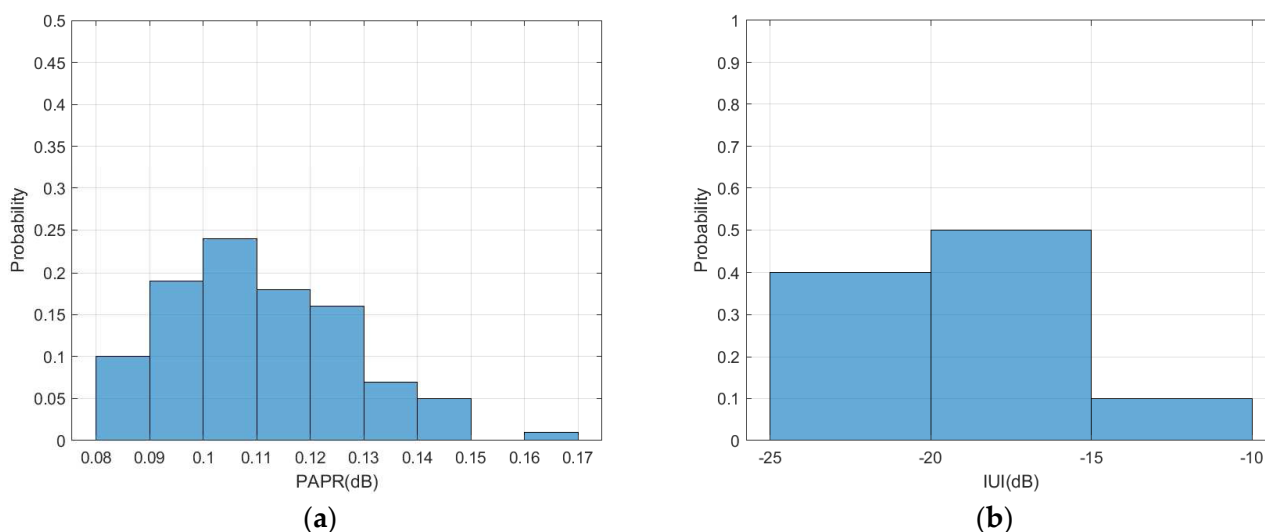


Figure 6. PAPR and IUI performance of Algorithm 2. (a) PAPR performance of Algorithm 2 under QPSK when $M = 64$; (b) IUI performance of Algorithm 2 under 16 QAM when $M = 64$.

5. Conclusions

In this work, for the massive multiuser MIMO-OFDM architecture in the angular domain, the precoding-based PAPR reduction algorithms are investigated. Here, we analyze the system performance in terms of SER, PAPR reduction efficiency, and the IUI using the EM-TGM-GAMP scheme and the proposed OADMM technique. By utilizing the huge MIMO-OFDM-ADMA framework, the high PAPR issue is minimized to no more than 0.18 dB. Moreover, the SER is about 10^{-5} dB when the OADMM algorithm is used. Numerical results verify the efficient performance of the proposed precoding-based PAPR reduction technique in terms of the SER, PAPR reduction, and IUI performance.

Author Contributions: Conceptualization, T.L.; methodology, T.L.; software, T.L.; validation, T.L.; formal analysis, T.L.; investigation, T.L.; resources, T.L.; data curation, T.L.; writing—original draft preparation, T.L.; writing—review and editing, T.L., X.W., Y.X. and X.Y.; visualization, T.L.; supervision, T.L.; project administration, T.L.; funding acquisition, T.L. and X.Y. All authors have read and agreed to the published version of the manuscript.

Funding: This research was funded by NSFC (62101274), Jiangsu NSF (BK20210640), and Shanghai Pujiang Program (22PJ1403100).

Data Availability Statement: Data sharing is not applicable to this article.

Acknowledgments: The authors would like to thank all authors of their fundings.

Conflicts of Interest: The authors declare no conflict of interest.

References

- Pereira de Figueiredo, F.A. An overview of massive MIMO for 5G and 6G. *IEEE Lat. Am. Trans.* **2022**, *20*, 931–940. [[CrossRef](#)]
- Jiang, H.; Xiong, B.; Zhang, H.; Basar, E. Hybrid far- and near-field modeling for reconfigurable intelligent surface assisted V2V channels: A sub-array partition based approach. *IEEE Trans. Wirel. Commun.* **2023**. [[CrossRef](#)]
- Basar, E. Reconfigurable intelligent surface-based index modulation: A new beyond MIMO paradigm for 6G. *IEEE Trans. Commun.* **2020**, *68*, 3187–3196. [[CrossRef](#)]
- Jeon, J.; Lee, G.; Ibrahim, A.A.I.; Yuan, J.; Xu, G.; Cho, J.; Onggosanusi, E.; Kim, Y.; Lee, J.; Zhang, J.C. MIMO evolution toward 6G: Modular massive MIMO in low-frequency bands. *IEEE Commun. Mag.* **2021**, *59*, 52–58. [[CrossRef](#)]
- Shlezing, N.; Alexandropoulos, G.C.; Imani, M.F.; Eldar, Y.C.; Smith, D.R. Dynamic metasurface antennas for 6G extreme massive MIMO communications. *IEEE Wirel. Commun.* **2021**, *28*, 106–113. [[CrossRef](#)]
- He, H.; Yu, X.; Zhang, J.; Song, S.; Letaief, K.B. Cell-free massive MIMO for 6G wireless communication networks. *J. Commun. Inf. Net.* **2021**, *6*, 321–335. [[CrossRef](#)]

7. Chen, S.; Zhang, J.; Jin, Y.; Ai, B. Wireless powered IoE for 6G: Massive access meets scalable cell-free massive MIMO. *China Commun.* **2020**, *17*, 92–109. [[CrossRef](#)]
8. Bai, L.; Huang, Z.; Zhang, X.; Cheng, X. A non-stationary 3D model for 6G massive MIMO mmWave UAV channels. *IEEE Trans. Wirel. Commun.* **2022**, *21*, 4325–4339. [[CrossRef](#)]
9. Wang, Y.; Gao, Z.; Zheng, D.; Chen, S.; Gunduz, D.; Poor, H.V. Transformer-empowered 6G intelligent networks: From massive MIMO processing to semantic communication. *IEEE Wirel. Commun.* **2022**. [[CrossRef](#)]
10. Cui, M.; Wu, Z.; Lu, Y.; Wei, X.; Dai, L. Near-field MIMO communications for 6G: Fundamentals, challenges, potentials, and future directions. *IEEE Commun. Mag.* **2023**, *61*, 40–46. [[CrossRef](#)]
11. Guan, K.; Yi, H.; He, D.; Ai, B.; Zhong, Z. Towards 6G: Paradigm of Realistic Terahertz Channel Modeling. *China Commun.* **2021**, *18*, 1–18. [[CrossRef](#)]
12. Guan, K.; Ai, B.; Peng, B.; He, D.; Li, G.; Yang, J.; Zhong, Z.; Kuerner, T. Towards realistic high-speed train channels at 5G millimeter-wave band—Part I: Paradigm, Significance Analysis, and Scenario Reconstruction. *IEEE Trans. Veh. Technol.* **2018**, *67*, 9112–9128. [[CrossRef](#)]
13. Papazafeiropoulos, A. Joint spatial division and multiplexing for FDD in intelligent reflecting surface-assisted Massive MIMO systems. *IEEE Trans. Veh. Technol.* **2022**, *71*, 10754–10769. [[CrossRef](#)]
14. Jiang, H.; Xiong, B.; Zhang, H.; Basar, E. Physics-based 3D end-to-end modeling for double-RISs assisted non-stationary UAV-to-ground communication channels. *IEEE Trans. Commun.* **2023**, *71*, 4247–4261. [[CrossRef](#)]
15. Jia, R.; Chen, X.; Qi, Q.; Lin, H. Massive beam-division multiple access for B5G cellular internet of things. *IEEE Internet Things J.* **2020**, *7*, 2386–2396. [[CrossRef](#)]
16. Yuan, H.; Wang, X.; Yang, K.; An, J. Hybrid precoding for cluster-based multi-carrier beam division multiple access in terahertz wireless communications. *China Commun.* **2021**, *18*, 81–92. [[CrossRef](#)]
17. Li, Y.; Mohsan, S.A.H.; Chen, X.; Tehseen, R.; Li, S.; Wang, J. Research on power allocation in multiple-beam space division access based on NOMA for underwater optical communication. *Sensors* **2023**, *23*, 1746. [[CrossRef](#)] [[PubMed](#)]
18. Ding, Z. Potentials and limits of using preconfigured spatial beams as bandwidth resources: Beam selection versus beam aggregation. *IEEE Wirel. Commun. Lett.* **2022**, *11*, 2575–2579. [[CrossRef](#)]
19. Li, R.; Yan, H.; Cabric, D. Rainbow-link: Beam-alignment-free and grant-free mmW multiple access using true-time-delay array. *IEEE J. Select. Areas Commun.* **2022**, *40*, 1692–1705. [[CrossRef](#)]
20. Zhu, L.; Xiao, Z.; Xia, X.G.; Wu, D.O. Millimeter-wave communications with non-orthogonal multiple access for B5G/6G. *IEEE Access* **2019**, *7*, 116123–116132. [[CrossRef](#)]
21. Mu, X.; Liu, Y.; Guo, L.; Lin, J.; Schober, R. Joint deployment and multiple access design for intelligent reflecting surface assisted networks. *IEEE Trans. Wirel. Commun.* **2021**, *20*, 6648–6664. [[CrossRef](#)]
22. Wu, Y.; Gao, X.; Zhou, S.; Yang, W.; Polyanskiy, Y.; Caire, G. Massive access for future wireless communication systems. *IEEE Wirel. Commun.* **2020**, *27*, 148–156. [[CrossRef](#)]
23. Lin, H.; Gao, F.; Jin, S.; Li, G.Y. A new view of multi-user hybrid massive MIMO: Non-orthogonal angle division multiple access. *IEEE J. Select. Areas Commun.* **2017**, *35*, 2268–2280. [[CrossRef](#)]
24. Liu, X.; Sha, J.; Xie, H.; Gao, F.; Jin, S.; Zhang, Z.; You, X.; Zhang, C. Efficient channel estimator with angle-division multiple access. *IEEE Trans. Circuits Syst. I Regul. Pap.* **2019**, *66*, 708–718. [[CrossRef](#)]
25. Wang, B.; Si, Q.; Jin, M. A novel tone reservation scheme based on deep learning for PAPR reduction in OFDM systems. *IEEE Commun. Lett.* **2020**, *24*, 1271–1274. [[CrossRef](#)]
26. Wang, J.; Lv, X.; Wu, W. SCR-based tone reservation schemes with fast convergence for PAPR reduction in OFDM system. *IEEE Wirel. Commun. Lett.* **2019**, *8*, 624–627. [[CrossRef](#)]
27. DelMarco, S.P. A constrained optimization approach to compander design for OFDM PAPR reduction. *IEEE Trans. Broadcast.* **2017**, *64*, 307–318. [[CrossRef](#)]
28. Rateb, A.M.; Labana, M. An optimal low complexity PAPR reduction technique for next generation OFDM systems. *IEEE Access* **2019**, *7*, 16406–16420. [[CrossRef](#)]
29. Huang, Y.; Hu, S.; Ma, S.; Liu, Z.; Xiao, M. Designing low-PAPR waveform for OFDM-based radcom systems. *IEEE Trans. Wirel. Commun.* **2022**, *21*, 6979–6993. [[CrossRef](#)]
30. Aghdam, M.H.; Sharifi, A.A. PAPR reduction in OFDM systems: An efficient PTS approach based on particle swarm optimization. *ICT Express* **2019**, *5*, 178–181. [[CrossRef](#)]
31. Padarti, V.K.; Rao, N.V. Adaptive SOICAF algorithm for PAPR mitigation in OFDM systems. *Wirel. Pers. Commun.* **2020**, *113*, 927–943. [[CrossRef](#)]
32. Sarowa, S.; Kumar, N.; Agrawal, S.; Sohi, B.S. Evolution of PAPR reduction techniques: A wavelet based OFDM approach. *Wirel. Pers. Commun.* **2020**, *115*, 1565–1588. [[CrossRef](#)]
33. Liang, R.; Li, H.; Zhang, W.; Liu, C.; Guo, Y. An efficient nonlinear quantized constant envelope precoding for Massive MU-MIMO systems. *IEEE Syst. J.* **2022**. [[CrossRef](#)]
34. Tan, J.; Xiao, Y.; Dan, L.; Xiang, W. Efficient LLR approximation for coded constant envelop OFDM. *IEEE Trans. Veh. Technol.* **2023**, *72*, 6194–6208. [[CrossRef](#)]
35. Berekhi, A.; Sedaghat, M.A.; Muller, R.R. Precoding via Approximate Message Passing with Instantaneous Signal Constraints. Available online: <https://arxiv.org/abs/1801.02442> (accessed on 8 January 2018).

36. Mezghani, A.; Heath, R.W. Massive MIMO precoding and spectral shaping with low resolution phase-only DACs and active constellation extension. *IEEE Trans. Wirel. Commun.* **2022**, *21*, 5265–5278. [[CrossRef](#)]
37. Bao, H.; Fang, J.; Chen, Z.; Li, H.; Li, S. An efficient bayesian PAPR reduction method for OFDM-based massive MIMO systems. *IEEE Trans. Wirel. Commun.* **2016**, *15*, 4183–4195. [[CrossRef](#)]

Disclaimer/Publisher’s Note: The statements, opinions and data contained in all publications are solely those of the individual author(s) and contributor(s) and not of MDPI and/or the editor(s). MDPI and/or the editor(s) disclaim responsibility for any injury to people or property resulting from any ideas, methods, instructions or products referred to in the content.